Available online at www.sciencedirect.com
SCIENCE DIRECT®
Physica A 342 (2004) 428–446
PHYSICA A
www.elsevier.com/locate/physa

Concerning maximal packing arrangements of binary disk mixtures

O.U. Uche[a,1], F.H. Stillinger[b,2], S. Torquato[b,c,*]

[a] *Department of Chemical Engineering, Princeton University, Princeton, NJ 08544, USA*
[b] *Department of Chemistry, Princeton University, Princeton, NJ 08544, USA*
[c] *Department of Chemical Engineering, Princeton Materials Institute, Princeton University, Princeton, NJ 08544, USA*

Abstract

The determination of the maximal packing arrangements of two-dimensional, binary hard disks of radii R_S and R_L (with $R_S \leqslant R_L$) for sufficiently small R_S amounts to finding the optimal arrangement of the small disks within a *tricusp*: the nonconvex cavity between three close-packed large disks. We present a particle-growth Monte Carlo algorithm for the generation of geometric packings of equi-sized hard disks within such a tricusp. The first 19 members of an infinite sequence of maximal density structures thus produced are reported. In addition, the Monte Carlo algorithm is applied to the geometric packing of disks within a flat-sided equilateral triangle and compared to published results for that packing problem. We perform an analysis of geometric properties of the packings, e.g. packing fractions and symmetries of structures confined to both containers. Interestingly, we find a non-monotonic increase in the packing fraction with increasing number of disks packed within both the flat-sided triangle and tricusp. It is important to note that for disk packings within a flat-sided equilateral triangle, this non-monotonic behavior of the packing fraction had not been reported in previously published works. For the flat-sided equilateral triangle, local maxima occur at the triangular integers $N_S = 1, 3, 6, 10, 15 \ldots$, as well as $N_S = 12$, where N_S is the number of disks in each packing. However, local maxima for packings within the tricusp exist at $N_S = 1, 3, 6, 10, 18 \ldots$. Finally, we analyze the asymptotic approach to the upper bound on the packing fraction of the infinite sequence of maximal structures of disks confined to the tricusp.

PACS: 05.20.−y; 05.70.Fh; 61.50.Ah

Keywords: Maximal packings; Binary hard-disk mixtures; Polydispersity; Rattlers; Tricusp; Packing fraction

* Corresponding author. Tel.: +1-609-258-3341; fax: +1-609-258-6878.
E-mail address: torquato@princeton.edu (S. Torquato).

[1] Supported by the US Department of Energy Computational Science Graduate Fellowship.
[2] Supported in part by the Petroleum Research Fund as administered by the American Chemical Society, and by the MRSEC Grant at Princeton University, NSF-DMR-0213706.

0378-4371/$ - see front matter © 2004 Elsevier B.V. All rights reserved.
doi:10.1016/j.physa.2004.05.082

1. Introduction

Due to the fact that the structure of a many-particle system is often determined primarily by repulsive interactions, hard-sphere packings serve as useful models for a variety of systems. Examples include simple liquids, colloidal dispersions, fiber-reinforced composites, granular media, and glasses [1–5]. Hard spheres only interact when they are in contact with each other, resulting in an infinite repulsion that reflects their impenetrable core [6]. We will deal with hard, circular disks in two dimensions for the purposes of this paper and reserve the three-dimensional extension, which differs from the present two-dimensional problem by virtue of a percolating interstitial space, for later consideration.

Polydispersity in particle size is a fundamental feature of the microstructure of a wide class of many-particle systems. In two dimensions, a monodisperse disk system crystallizes in a triangular close-packed (TCP) lattice with a packing (covering) fraction, $\phi = \pi/\sqrt{12} \approx 0.906899\ldots$; in general, one is able to exceed this packing fraction by introducing some polydispersity into the system of congruent (equi-sized) disks. Intuitively, the wider the distribution of available disk sizes, the higher the packing efficiency of the system in question as the disk sizes range to the infinitesimally small. However, our studies indicate that this is not necessarily the case.

The effect of polydispersity on microstructure and the effective properties can be dramatic and thus is of great interest. A particular case is one in which particles with conducting properties are prevented from forming a connected network as a result of the relative size and composition of surrounding non-conducting particles. Evidently, the resulting arrangement will have a substantial effect on the binary system properties as compared to the properties of the individual monodisperse systems [6]. Another case in point involves the dissolution of a crystal comprised of polydisperse disks. The large disks will restrict the solubility of the crystal in the solvent [7].

Real-world applications of maximal, polydisperse disk structures include optimal packing of cables in a conduit (viewed in cross section). In addition, maximal ordered arrangements have been studied in the investigation of the phase diagram of two-dimensional binary mixtures of hard disks [8]. That investigation is accomplished by minimizing the area per particle for each given alloy. Alternatively, a particular area of interest for engineers concerns fluid flow in packed bed reactors. An extension of our research to three dimensions should provide information on the optimal packing of spherical catalyst pellets, which can aid in studying the nature of flow patterns and reaction through the reactor.

The understanding of hard-particle packings in confined regions of space [9] is an important subject of applied interest. In particular, the subject of capillary condensation which involves the liquid–gas transition of a fluid in a restricted cavity has been explored for parallel walls [10] and slit-like pores [11]. Freezing in hard-particle systems confined to circular cavities [12] and parallel plates [13] has also been studied. The confining walls play an important role in modifying the thermodynamic fluctuations in the fluid, leading to observable changes in its behavior. Even though the structures formed at freezing are not maximally dense, understanding maximal packing arrangements in confined regions is fundamental to comprehending freezing in such cavities.

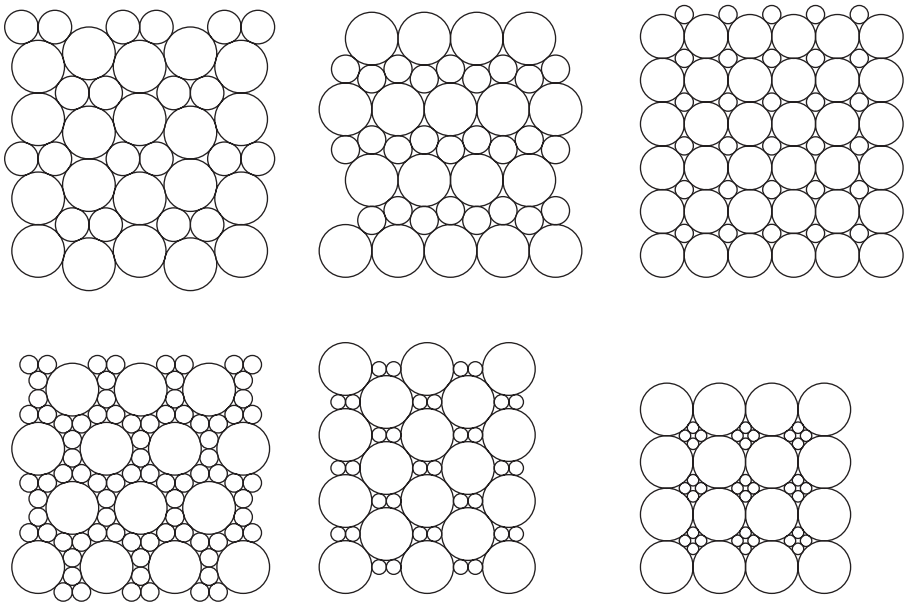

Fig. 1. Six two-dimensional binary structures for which $\alpha > 0.2$. These structures were originally reported by Fejes Tóth [21].

It is also of interest to note that the Apollonian packing of disks provides another special class of confined disk packings [14].

Several studies have investigated disordered, polydisperse systems in two- and three-dimensional space [15–17]. Particularly in two dimensions, results show that for a radius ratio (of large to small) less than five, the density of a binary disk mixture is virtually independent of polydispersity and remains constant at a packing fraction, $\phi \approx 0.84$ [18]. This value for the packing fraction is significantly lower than that associated with ordered packings of comparable polydispersity. Similarly, it is well known that congruent spheres are optimally packed in a face-centered cubic or hexagonal close-packed arrangement [19,20]. Clearly, this reveals that a high degree of order must be imparted to a system so as to generate maximally dense structures.

In this paper, we consider binary packings of disks, i.e., two-dimensional disks of two different radii, R_S and R_L, where $R_S \leqslant R_L$. Ideally, it is desired to obtain the maximal packing fraction, $\phi_{\max}$, for given values of $\alpha = R_S/R_L$ and the mole fraction of disks of size R_S, x_S. Specifically, $x_S = N_S/(N_S + N_L)$, where N_S and N_L are the populations of smaller and larger disks, respectively, in the lattice of choice. The packing efficiency of monodisperse hard-disk arrangements can be improved by introducing polydispersity and order. In particular, Fejes Tóth [21] has reported several two-dimensional binary structures of high packing efficiency for $\alpha \geqslant 0.154701\ldots$ (see Fig. 1 and Table 1).

Our research was motivated by a desire to discover more dense binary disk arrangements than those presented by Fejes Tóth [21]. This amounts to finding the maximal

Table 1
Relevant parameters for the binary structures displayed in Fig. 1

Structure	α	x_S	ϕ
Top left panel	0.637247	1/2	0.910951
Top center panel	0.533296	2/3	0.914180
Top right panel	0.414214	1/2	0.920151
Bottom left panel	0.349198	6/7	0.926192
Bottom center panel	0.280776	2/3	0.929952
Bottom right panel	0.216845	4/5	0.933122

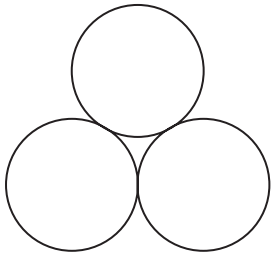

Fig. 2. Three identical disks in a triangular close-packed arrangement. The cavity within this close-packed triad of disks is termed a tricusp.

packing arrangements of the small disks within the cavities of the TCP lattice of the large disks. Thus, the problem becomes one of determining the optimal arrangement of equi-sized disks within a *tricusp*: the non-convex cavity between three close-packed large disks (see Fig. 2). The binary structures are generated by making use of our particle-growth Monte Carlo algorithm. These optimal structures have packing fractions between that of the single-species TCP lattice value $\phi_{tl} = \pi/\sqrt{12} \approx 0.906899\ldots$ and the maximal allowable value of $\phi_{tl} + \phi_{tl}(1-\phi_{tl}) \approx 0.991332\ldots$. Ultimately, we seek the best estimate to the function $\phi_{max}(\alpha, x_S)$ over the range $0 < \alpha \leqslant 0.154701\ldots$ and $0 < x_S \leqslant 1$.

In Section 2, we describe the particle-growth Monte Carlo algorithm for generation of maximal packing arrangements. In Section 3, we tabulate and illustrate our findings. Upper bounds for the packing fraction associated with varying values of α are also discussed in that section. We compare packing structures and geometric properties for the tricusp and flat-sided equilateral triangle in Section 4. In the concluding section, we discuss jamming categories for the arrangements. In addition, some remarks have been directed to the occurrence of ordered arrangements in quasicrystals and our conclusions have been summarized. A derivation of the asymptotic upper bound on the packing fraction is presented in Appendix A.

2. Numerical procedure

Monte Carlo simulations are proven methods for obtaining representative configurations of molecules in equilibrium [22]. However, we note that for binary systems, there is an inherent inefficiency associated with these methods. In particular, selection of move sizes for the particles is important. Reasonable displacements for the small particles may not be so reasonable for the large particles. As large displacements will provide higher probability for overlap of the large disks which in turn lead to rejections of these trial moves, we are constrained to use small displacements. However, the choice of small displacements to allow for rearrangements of all disks will force the system to evolve slowly [6,22].

Focusing on displacing only the small particles circumvents the above issue. In effect, this modified approach for the generation of geometric packing structures involves performing Monte Carlo (MC) simulations of disks within the container of choice, a tricusp. The disks are grown in size during the simulation. The algorithm for this MC simulation is as follows:

- *Initial setup*: The container perimeter is specified. The disks are initiated as very small particles. Position coordinates are assigned to all disks using a *random sequential addition* (RSA) method [6]. The disks are randomly distributed subject to the condition that:
  - There is no overlap between any of the particles in the system.
  - All particles must occupy the interior of simulation box/container.
- Proceed with MC simulation. During each MC cycle, potential displacements of two types occur:
  - First, attempt moving each disk (in sequence) such that its displacement is less than or equal to the specified maximum step size. The direction of displacement is entirely random. If a particular disk cannot be moved over the random displacement, skip the disk and attempt moving the next disk.
    The simulation is performed in three stages during which different step sizes are implemented. All three step sizes are proportional to the initial diameter of the disks, $D_{S,0}$. During the initial stage, the step size is assigned a value of $10^{-2}D_{S,0}$. The step size is reduced to a tenth of its value in the previous stage for the latter stages. In other words, the intermediate stage step size is $10^{-3}D_{S,0}$ and the step size in the final stage is $10^{-4}D_{S,0}$.
  - Second, attempt growth of disks. The growth increment is specified as a fixed fraction of the present disk diameter. In our simulation, we have used a growth increment of 0.025%. To keep sizes uniform, either grow all or none of the particles during each cycle. Ensure all particles have room for growth for the specified growth increment by displacing nearest neighbors, if necessary:
    If two particles are sufficiently close that an incremental change in size will result in overlap, randomly displace both particles in opposite directions along the line of centers until there is enough room for growth.
    If a particle is sufficiently close to the container boundary that an incremental size change will result in the particle crossing the boundary, randomly displace only that particle towards the interior of the container.

Table 2
Comparison of maximum separation distances for optimal packings of disks within a flat-sided equilateral triangle

N_S	d_{N_S}	$d^*_{N_S}$
3	0.999894	1.000000
4	0.577323	0.577350
5	0.499836	0.500000
6	0.499921	0.500000
7	0.366025	0.366025
8	0.343016	0.343070
9	0.333288	0.333333
10	0.333258	0.333333
11	0.275080	0.275255
12	0.267534	0.267949
13	0.251715	0.251813
14	0.249857	0.250000
15	0.249885	0.250000

N_S is the number of disks arranged in the equilateral triangle, d_{N_S} is the maximum separation distance of packings obtained by the particle-growth MC algorithm, and $d^*_{N_S}$ is the maximum separation distance reported by Melissen [23].

- Repeat previous step until the hard-particle system approaches its jammed state. The jammed state is reached when the average gap between neighboring disks is less than $10^{-5}R_S$ where R_S is the final disk radius.

The particle-growth Monte Carlo algorithm can be extended to any simulation space of choice. In Table 2, we compare results generated by the above algorithm to reported results from Melissen [23]. In both cases, the maximum separation distance d_{N_S} of optimal packings of two-dimensional disks within a flat-sided equilateral triangle are presented. d_{N_S} is defined as the ratio of the disk diameter to the side length of the smallest equilateral triangle that contains all particle centers. The choice of measure, d_{N_S}, is consistent with previously published conventions for disk packings within a flat-sided equilateral triangle. The reader should note that the bounding triangle we use in our MC routine contains the entirety of the disks, not just their centers as in the Melissen calculations. Conversion between these conventions is not a trivial matter and can amplify discrepancy between pairs of entries in Table 2. However, it is obvious that results generated from our algorithm have good agreement with the published data. Small differences in d_{N_S} between both sets of data can be reduced by executing our simulation at even lower growth rates and with a tighter jamming criterion than specified above.

3. Results

3.1. Maximal packings in the tricusp

The basic rationale in constructing the maximal structures lies in the knowledge that these packings can be formed within an original arrangement of the equi-sized

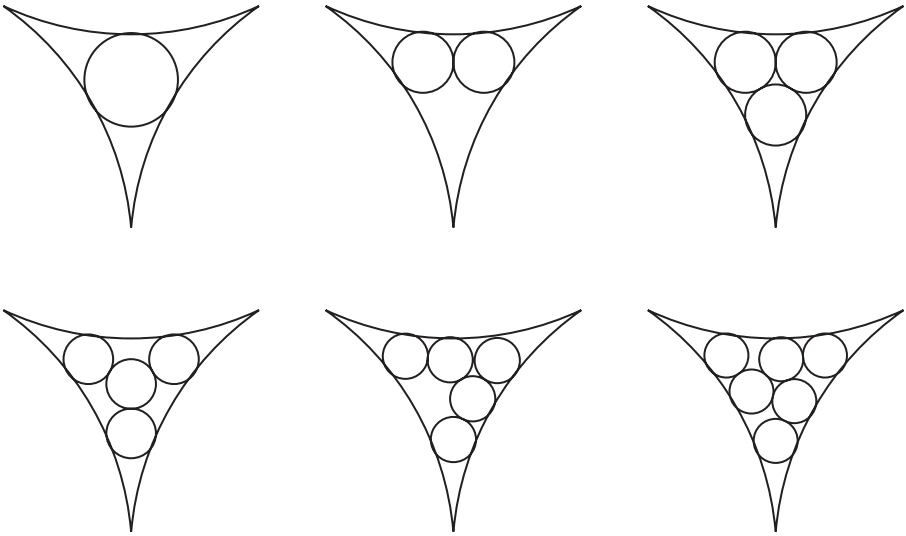

Fig. 3. Structures for $N_S = 1$–6 of an infinite series of packing arrangements in which small disks are optimally located within the cavity of three large disks arranged in the TCP lattice. These maximal structures were generated via the particle-growth MC algorithm.

larger disks in the TCP lattice. Increasing numbers of smaller disks are then inserted in optimal arrangements within the tricusps formed by the larger disks. We make use of the algorithm presented in Section 2 for the generation of these maximal structures. We perform Monte Carlo simulations of N_S small disks within the tricusp of large disks. It should be noted that the effective value of N_L is 1/2 when considering the N_S small disks arranged in a single tricusp because each of the three large disks is part of six tricusps in the TCP lattice. We present the first 19 members of an infinite sequence, with larger and larger numbers of smaller and smaller disks filling the interstices of the triangular large-disk lattice. Structures generated via this method are displayed in Figs. 3–6. Relevant parameters for these structures are reported in Table 3.

The packing fraction for this infinite sequence approaches the limiting value [6]

$$\phi_{limit} = \phi_{tl} + (1 - \phi_{tl})\phi_{tl} \approx 0.991332\ldots\ . \tag{1}$$

It should be noted that the packing fraction does not monotonically increase with decreasing radius ratio (increasing N_S) for this infinite sequence. In fact, local maxima in the packing fraction exist at $N_S = 1, 3, 6, 10, 18, \ldots$ for structures of this type. Initially, this observation may seem counter-intuitive, but results suggest that the local maxima are associated with a relatively high degree of symmetry (see Table 4).

Several of the arrangements, e.g. those corresponding to $N_S = 2, 5, 6$, and 7 can have varying orientation. This can introduce a lack of periodicity in an extended binary crystal. Specifically, the five small disks in the bottom center panel of Fig. 3 can be oriented in three different ways within the large-disk tricusp. In view of the fact that the small disks can be independently arranged in each of the tricusps, these

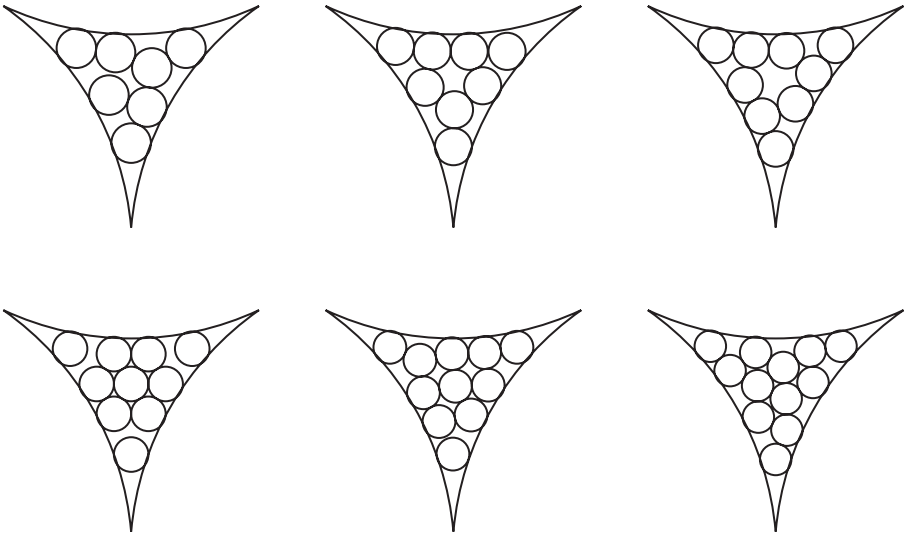

Fig. 4. As in Fig. 3, except $N_S = 7$–12.

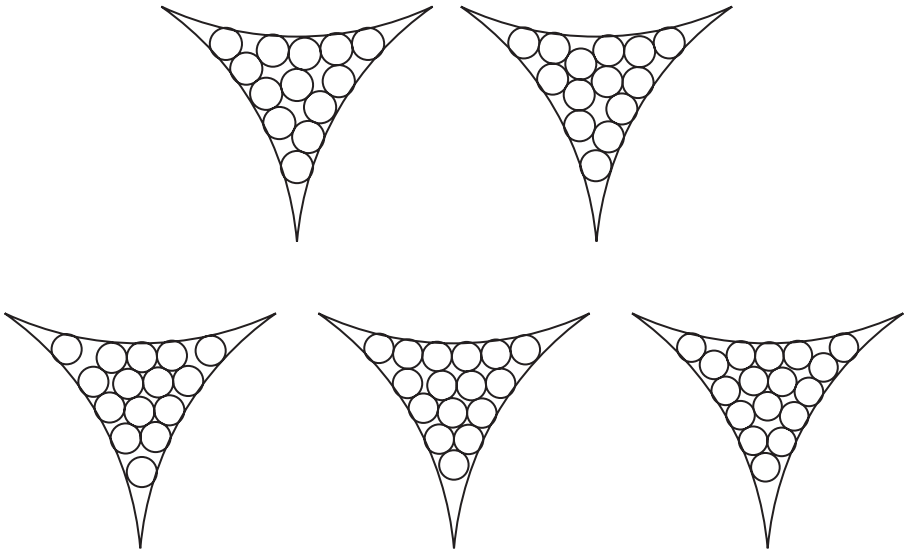

Fig. 5. As in Fig. 3, except $N_S = 13$–17.

structures may be viewed as local arrangements in a degenerate family of packings that possess local orientational disorder. Also, in two-dimensional particle packings, disks that are not necessarily in contact with three or more other disks are referred to as *rattlers*. In particular, the number of rattlers that occur in the maximally dense

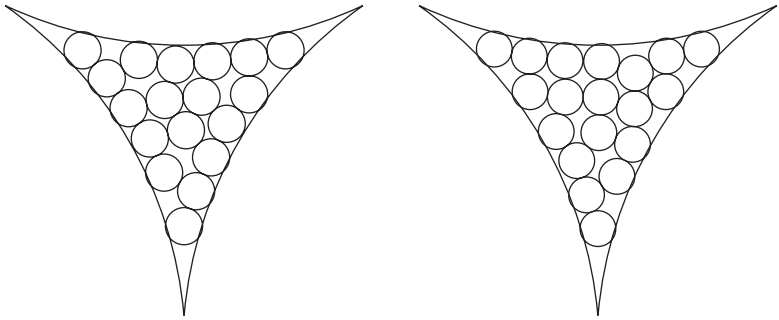

Fig. 6. As in Fig. 3, except $N_S = 18$ and 19.

Table 3
Relevant geometric parameters for the structures displayed in Figs. 3–6

N_S	α	x_S	ϕ
1	0.154701	2/3	0.950308
2	0.101020	4/5	0.943919
3	0.101020	6/7	0.962458
4	0.082035	8/9	0.955726
5	0.074624	10/11	0.957403
6	0.072819	12/13	0.964607
7	0.065372	14/15	0.961159
8	0.061339	16/17	0.961494
9	0.058868	18/19	0.963709
10	0.057188	20/21	0.966219
11	0.054269	22/23	0.965659
12	0.052078	24/25	0.965931
13	0.050135	26/27	0.966167
14	0.048341	28/29	0.966240
15	0.046995	30/31	0.966988
16	0.045895	32/33	0.968028
17	0.044549	34/35	0.968094
18	0.043863	36/37	0.969714
19	0.042218	38/39	0.968324

Reported data includes number of small disks within the tricusp N_S, radius ratio α, mole fraction of small disks $x_S = 2N_S/(2N_S + 1)$, and the unit cell packing fraction ϕ.

packings for $N_S = 7, 10, 15$, and 17 are $1, 3, 3$, and 1, respectively. Table 4 shows a classification of the jammed disk subsets displayed in Figs. 3–6 in various symmetry categories.

The effect of the choice of step size on the numerical accuracy of the packing fraction of the maximally dense structures should not be underestimated. In Table 5, we report the percent error in the packing fraction for different values of the step size for the maximally dense structure of $N_S = 6$. For this case, an exact value of the packing fraction ($\phi = 0.964607\ldots$) can be obtained by algebraic techniques. Clearly, the

Table 4
Classification of the symmetry of jammed disk subsets displayed in Figs. 3–6

Full 3-fold rotational and reflection symmetry	$N_S = 1, 3, 4, 10$
3-fold rotational symmetry (but no reflection)	$N_S = 6, 9, 12, 13, 18$
Reflection (but no rotational symmetry)	$N_S = 2, 5, 7, 8$
No symmetry	$N_S = 11, 14, 15, 16, 17, 19$

Note that in assigning these symmetries, *rattler* disks have been placed at their average positions over their respective displacement domains.

Table 5
The effect of step size on the packing fraction for the maximally dense structure of $N_S = 6$

Step size/$D_{S,0}$	ϕ	Percent error in ϕ
1.01	0.964267	0.035248
0.5	0.964393	0.022167
0.1	0.964376	0.023938
0.05	0.964484	0.012749
0.01	0.964543	0.006642
$0.01 \rightarrow 0.001 \rightarrow 0.0001$	0.964603	0.000400

Table 6
Detection frequency of the maximal structures displayed in Figs. 4–6

N_S	ϕ	Detection frequency
8	0.961494	0.540000
9	0.963709	0.360000
10	0.966219	0.600000
11	0.965659	0.560000
12	0.965931	0.265306
13	0.966167	0.215686
14	0.966240	0.333333
15	0.966988	0.160000
16	0.968028	0.100000
17	0.968094	0.140000
18	0.969714	0.211538
19	0.968324	0.080000

sequentially reduced step size discussed in Section 2 yields the most accurate packing fraction.

Fifty or more realizations were generated for each value of N_S using random initial conditions. Table 6 presents the detection frequency of the maximally dense structures for $N_S = 8, 9, \ldots, 19$. The decreasing frequency of occurrence of the maximal structures as N_S increases is apparent. There is a range in ϕ over all jammed structures for a fixed N_S. For the most part, we find that the range in ϕ is reduced as N_S is increased. For example, the least dense jammed configuration for $N_S = 6$ yields a packing fraction

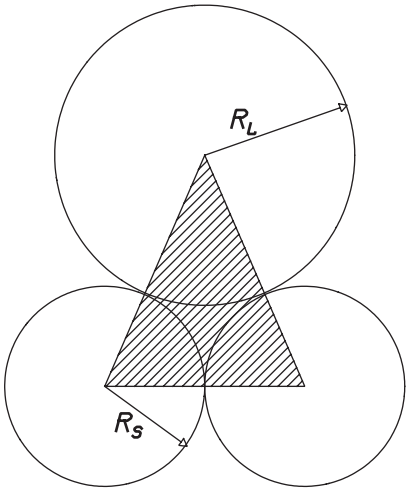

Fig. 7. One large disk and two small disks in mutual contact. The intersection of the shaded triangle with the three disks yields the local packing fraction.

that is 98.8% of its maximal packing fraction. In contrast, the least dense jammed packing has a packing fraction that is 99.4% of the maximal value for $N_S = 18$.

3.2. Upper bound on the packing fraction

In binary systems, numerical computations suggest that the packing fraction is bounded above by the case of one large disk and two small disks, mutually touching one another as shown in Fig. 7 [21]. This simple bound $s(\alpha)$ can be expressed in the form:

$$s(\alpha) \cong \frac{\pi\alpha^2 + 2(1-\alpha^2)\arcsin(\alpha/1+\alpha)}{2\alpha(1+2\alpha)^{1/2}} \,. \tag{2}$$

As this is the best local packing arrangement, it follows that the global packing fraction is equal to or less than this best local packing fraction. The proof of this upper bound appears in Florian [24]. Eq. (2) is easily extended to multicomponent polydisperse packings in which case α is the ratio of the smallest disk radius to the largest disk radius. It should be noted that Eq. (2) predicts that $s(\alpha) \to 1$ as $\alpha \to 0$. In reality, as $\alpha \to 0$, a limiting value for the packing fraction, $\phi_{limit} = 0.991332\ldots$ is approached as noted above in Eq. (1).

We can obtain the upper bound on the packing fraction as a continuous function of N_S:

$$\phi^U(N_S) = \phi_{tl} + (1-\phi_{tl})\left(\frac{4\pi}{3^{1/2}}\,\frac{N_S}{\{(1+8N_S)^{1/2} + 2(3)^{1/2} - 3\}^2}\right) \,. \tag{3}$$

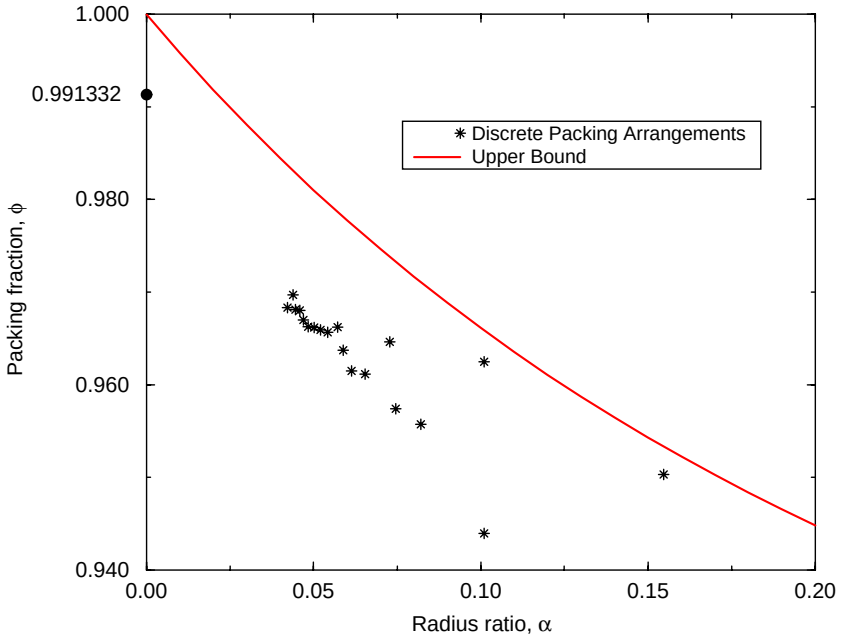

Fig. 8. Relationship between packing fraction ϕ and radius ratio α for periodic lattices built from structures in Figs. 3–6. Eq. (2) is plotted as a function of α for the upper bound curve.

As $\alpha \to 0$, the number of disks N_S that can be fitted within the tricusp becomes very large. However, the centers of these small disks are prevented from approaching the tricusp boundary any closer than the radius R_S. Consequently, an upper bound on the packing fraction ϕ^U for binary structures of this type as $N_S \to \infty$ is given by

$$\phi^U = \phi_{tl}\{1 + (1 - \phi_{tl})[1 - 0.328169 N_S^{-1/2} + O(N_S^{-1})]\} . \tag{4}$$

The above two equations are based on the assumption that the small disks are arranged in the TCP lattice within the tricusp. Details concerning the derivation of Eqs. (3) and (4) are provided in Appendix A.

Fig. 8 compares $s(\alpha)$ to the packing fractions for the structures depicted in Figs. 3–6. An important point that can immediately be observed from the plot is that the packing fractions of these maximal structures do not coincide with the upper bound. This suggests the possibility that polydisperse systems (three or more different particle sizes) are likely to approach the upper bound more closely. As $N_S \to \infty$ ($\alpha \to 0$), it should be noted that Eq. (3) becomes a more accurate estimate for the upper bound on ϕ than the upper bound derived by Florian [24]. Table 7 shows a comparison of the packing fraction for maximal structures for $N_S = 1, 3, 6, 10, 15$ and the corresponding upper bound from Eq. (3). We can expect packing structures generated within the tricusp to approach the limiting packing fraction ($\phi_{limit} = 0.991332\ldots$) for $N_S \to \infty$ slowly, as indicated by the reciprocal square root term in Eq. (4).

Table 7
Comparison of packing fraction for maximal structures generated within a curve-sided tricusp for $N_S = 1, 3, 6, 10, 15$

N_S	ϕ	$\phi^U(N_S)$
1	0.950308	0.963195
3	0.962458	0.974761
6	0.964607	0.979626
10	0.966219	0.982291
15	0.966988	0.983969

4. Comparison to packings in the flat-sided equilateral triangle

In this section, we compare the packing structures and geometric properties of disks optimally packed entirely within two similar containers: the flat-sided equilateral triangle and the tricusp of large disks. The tricusp can be viewed as an equilateral triangle with curved sides.

In some cases, similar optimal packings appear for both the flat-sided equilateral triangle and the tricusp with small positional differences imposed by the curved boundaries in the latter case. For an example, see the six-disk arrangements displayed in Fig. 9. Note that upon going from the flat-sided triangle to the tricusp, the symmetry of the arrangement has been reduced. However, for other cases, the optimal structures differ markedly from each other. The five-disk arrangements shown in Fig. 10 display this behavior. Essentially, the curved sides of the tricusp (in the right panel) force the relocation of the shaded disk and convert it to a rattler.

In addition, we compare packing fractions of maximal structures for both simulation regions. The packing fraction ζ is the area occupied by the particles relative to the total area of the encompassing equilateral triangle or tricusp, respectively. Table 8 displays the relevant data. ζ_{flat} is the packing fraction for the packing arrangements associated with the flat-sided equilateral triangle and ζ_{curved} is the packing fraction for those structures within the tricusp. An inspection of Table 8 reveals that ζ_{flat} is consistently higher than ζ_{curved}. One would expect such behavior as the equilateral triangle possesses some unique characteristics. In particular, the flat sides of the equilateral triangle mimic the straight edges of disks in a tiered TCP arrangement. Also, the vertex angle of the equilateral triangle is identical to the angle between disks in a triangular close-packed arrangement. The curved edges of the tricusp do not possess the above properties, and hence lead to less efficient packings.

A point of note is that the flat-sided equilateral triangle shows the same kind of non-monotonic increase in area fraction ζ that we observed for the curved-sided structures in Section 3.1. However, the local maxima generally occur at different values of N_S. For the flat-sided equilateral triangle, they occur at $N_S = 1, 3, 6, 10, 12, 15\ldots$, while they exist at $N_S = 1, 3, 6, 10, 18\ldots$ for the curve-sided tricusp. The disparity shows the effect of dissimilar maximal structures induced at high N_S by the curved sides of the tricusp. We expect both cases involve infinite sequences of maxima, with mostly unequal N_S values.

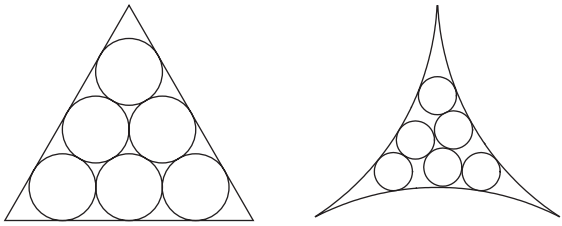

Fig. 9. Maximal packings of six disks in two different geometries. Left panel: equilateral triangle with flat sides. Right panel: equilateral triangle with curved sides.

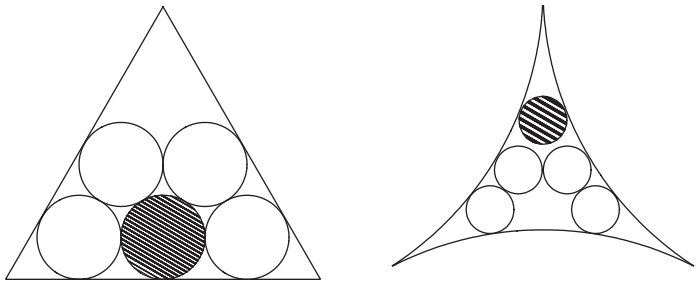

Fig. 10. Maximal packings of five disks in two different geometries. Left panel: equilateral triangle with flat sides. Right panel: equilateral triangle with curved sides. Note the large displacement of the shaded disk.

Table 8
Comparison of packing fractions for optimal structures generated within an equilateral triangle and within a curve-sided tricusp

N_S	ζ_{flat}	ζ_{curved}
3	0.728613	0.596456
4	0.604457	0.524441
5	0.650813	0.542464
6	0.781068	0.619840
7	0.686609	0.582805
8	0.671760	0.586406
9	0.728768	0.607638
10	0.809743	0.637159
11	0.692406	0.631144
12	0.726659	0.634057
13	0.724440	0.636601
14	0.772095	0.637389
15	0.827358	0.643424

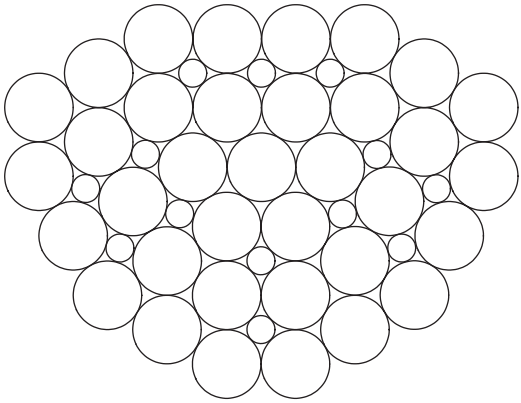

Fig. 11. Depiction of a quasicrystal. The radius ratio α for the quasicrystal is $\sqrt{2}-1$.

5. Discussion and conclusions

It is of interest to classify the optimal binary packings that we have found into their *jamming* categories. An individual particle is locally jammed if it has at least $d+1$ contacting neighbors not in the same semicircle or hemisphere, where d is the system dimension [6,25]. Clearly, this requirement is satisfied for the majority of configurations displayed in Figs. 3–6. Packings can be classified according to the following jamming categories: local, collective, and strict jamming [25,26]. A locally jammed packing is defined to be one in which all particles are locally jammed. A collectively jammed packing is a locally jammed packing in which no subset of particles can simultaneously be displaced so that the system unjams. A strictly jammed packing is collectively jammed and remains fixed despite attempted globally uniform area (volume)-maintaining deformations of the system boundary.

By virtue of the TCP lattice being a strictly jammed packing [25], all structures (TCP lattice of large disks and the small disk subset) in Figs. 3–6 are strictly jammed. For the subset of small disks within each tricusp, packings without rattlers are invariably locally jammed and are often collectively and strictly jammed. It should be noted that the likelihood of the incidence (though not necessarily the fraction) of rattlers may increase as α is reduced. The curved edges of the tricusp, as opposed to the straight edges of a triangle, contribute to the asymmetric structures. The presence of these isolated rattlers does not affect the jammed network as they can be removed without affecting the remainder of the network.

It is possible to create a non-periodic structure using disks of the same radius ratio ($\sqrt{2}-1$) as in the top right panel of Fig. 1 arranged in side-sharing modular units that are the filled squares, supplemented with close-packed triangles of large disks. Figs. 11 and 12 show the structure and its random tiling of squares and equilateral triangles. Such non-periodic structures are termed quasicrystals [27]; they possess long-range bond orientational order but lack spatial periodicity. Unlike crystals, quasicrystals do not have a simple unit cell that repeats infinitely in all directions but they do have

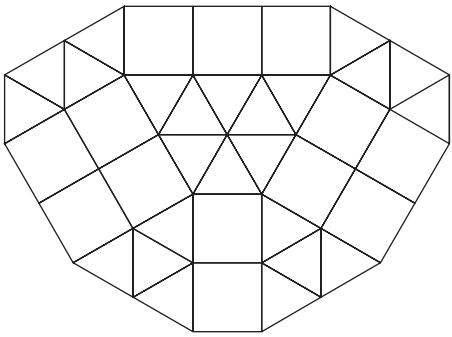

Fig. 12. Random square tiling composed of squares and triangles. The tiling is the underlying framework of the structure in Fig. 11.

a finite number of local patterns that repeat irregularly. Multi-component systems of metals form quasicrystals, and examples include alloys of Al, Mn, Fe, and Cr [28]. Many well-known two-dimensional quasicrystals resemble Penrose tilings, which use two different rhombi as basic building blocks to cover an infinite plane in complex, interlocking patterns [29,30]. Although we have no proof, it seems unlikely that other binary quasicrystals composed of internally jammed squares and triangles could exist for $\alpha < \sqrt{2} - 1$.

In conclusion, we have presented a particle-growth MC method for the generation of geometric disk packings in any container of choice. Our algorithm has been tested for packings within the flat-sided equilateral triangle and has yielded excellent agreement with published results [23]. In addition, the particle-growth MC algorithm has been used to generate the first 19 members of an infinite sequence of disk packings within the tricusp. We have compared the geometric properties of hard disks packed within the above two analogous geometric boundaries.

An important finding is the non-monotonic increase in the area fraction of optimal disks arranged within the interior of a flat-sided equilateral triangle and the tricusp of large disks. For the flat-sided triangle, the local maxima occur at $N_S = 1, 3, 6, 10, 12, 15\ldots$, whereas they appear at $N_S = 1, 3, 6, 10, 18\ldots$ for the curved-sided tricusp. For the latter case, we conjecture that this observation is due to the greater success of the appropriate number of disks to arrange themselves with a relatively high degree of symmetry within the curved walls. In addition, we derive an asymptotic upper bound on the packing fraction. We observe a slow approach to the upper bound suggesting that one would have to go to very high values of N_S to approach closely the limiting value of the packing fraction for structures formed within the tricusp.

Appendix A. An asymptotic upper bound to the packing fraction of disk packings

In this section, we present a derivation of an asymptotic upper bound to the packing fraction ζ^U of two-dimensional disks in an equilateral triangle or tricusp. It is the

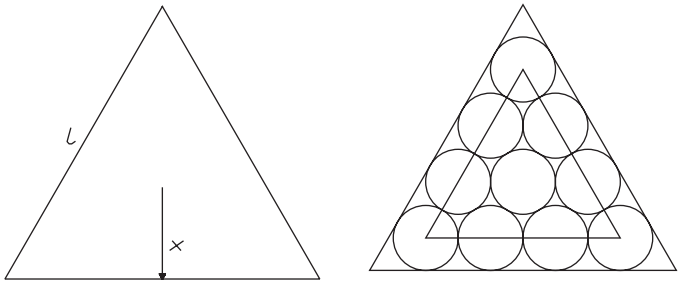

Fig. 13. Equilateral triangle representations. Left panel: depiction of relevant parameters. Right panel: packing of a triangular number of disks for $n = 4$ and $N = 10$.

assumption of the TCP arrangement in the following derivation that results in an upper bound to the packing fraction. As shown in the left panel of Fig. 13, the distance x to the edge from the centroid in the equilateral triangle, and the triangle area in terms of $x, A(x)$, are given by

$$x = \frac{l}{2(3)^{1/2}} , \tag{A.1}$$

$$A(x) = 3^{3/2}x^2 , \tag{A.2}$$

where l is the side length of the triangle. In order to maintain a perfect TCP arrangement, a triangular number of disks N is specified by

$$N = \tfrac{1}{2}\, n(n+1), \quad n = 1, 2, 3, \ldots . \tag{A.3}$$

For the inner triangle displayed in the right panel of Fig. 13, the edge length for an arbitrary triangular number of disks is

$$l(n) = 2(n-1)R_S . \tag{A.4}$$

As before, R_S is the disk radius. Combining Eqs. (A.1) and (A.2), we obtain

$$x(n) = \frac{(n-1)R_S}{3^{1/2}} . \tag{A.5}$$

By observing the right panel of Fig. 13, we note that the distance from the centroid to the edge of the outer triangle $\tilde{x}(n)$ is given by

$$\begin{aligned} \tilde{x}(n) &= x(n) + R_S \\ &= \left(\frac{n-1}{3^{1/2}} + 1 \right) R_S . \end{aligned} \tag{A.6}$$

The packing fraction of an arrangement of a triangular number of disks within the outer equilateral triangle is

$$\zeta^U(n) = \frac{\frac{1}{2}n(n+1)\pi R_S^2}{3^{3/2}[\tilde{x}(n)]^2}$$

$$= \frac{\frac{1}{2}n(n+1)\pi R_S^2}{(n+3^{1/2}-1)^2(3^{1/2}R_S^2)}$$

$$= \frac{\pi}{2(3)^{1/2}} \frac{n(n+1)}{(n+3^{1/2}-1)^2} . \tag{A.7}$$

A continuous function $\zeta^U(N)$ can be obtained by eliminating n from Eq. (A.7) in favor of N. This will provide an upper bound for both packing fractions of the equilateral triangle and tricusp. Thus, one obtains

$$\zeta^U(N) = \frac{4\pi}{3^{1/2}} \frac{N}{[(1+8N)^{1/2}+2(3)^{1/2}-3]^2} . \tag{A.8}$$

For large n, $\zeta^U(n)$ has the following behavior:

$$\zeta^U(n) = \frac{\pi}{2(3)^{1/2}} \frac{1+n^{-1}}{1+2(3^{1/2}-1)n^{-1}+2(2-3^{1/2})n^{-2}}$$

$$= \frac{\pi}{2(3)^{1/2}}\{1+[3-2(3)^{1/2}]n^{-1}+O(n^{-2})\} . \tag{A.9}$$

From Eq. (A.3), we note that

$$n^{-1} = \frac{2}{(1+8N)^{1/2}-1}$$

$$= (2N)^{-1/2}+O(N^{-1}) . \tag{A.10}$$

Combining Eqs. (A.9) and (A.10), we can obtain an expression for ζ^U as $N \to \infty$

$$\zeta^U = \frac{\pi}{2(3)^{1/2}}\{1-0.328169N^{-1/2}+O(N^{-1})\} . \tag{A.11}$$

Eqs. (3) and (4) can be obtained by, respectively, substituting Eqs. (A.8) and (A.11) in the following equation:

$$\phi^U = \phi_{tl} + (1-\phi_{tl})\zeta^U . \tag{A.12}$$

References

[1] H. Reiss, H.M. Ellerby, J.A. Manzanares, J. Phys. Chem. 100 (1996) 5970.
[2] W.B. Russel, D.A. Saville, W.R. Schowalter, Colloidal Dispersions, Cambridge University Press, Cambridge, England, 1989.
[3] S. Torquato, F. Lado, Proc. R. Soc. London A 417 (1988) 59.
[4] G. Metcalfe, T. Shinbrot, J.J. McCarthy, J.M. Ottino, Nature 374 (1995) 39.
[5] R. Zallen, The Physics of Amorphous Solids, Wiley, New York, 1983.
[6] S. Torquato, Random Heterogeneous Materials: Microstructure and Macroscopic Properties, Springer, New York, 2002.
[7] B. Mahan, R. Myers, University Chemistry, The Benjamin/Cummings Publishing Co., Inc, Menlo Park, CA, 1987.
[8] C.N. Likos, C.L. Henley, Philosophical Magazine B 1 (1993) 85.

[9] J. Klafter, J.M. Drake, Molecular Dynamics in Restricted Geometries, Wiley, New York, 1989.
[10] M. Schoen, D.J. Diestler, J.H. Cushman, J. Chem. Phys. 101 (1994) 6865.
[11] W. Rzysko, O. Pizio, S. Sokolowski, Intl. J. Modern Phys. C 10 (1999) 891.
[12] Z.T. Nemeth, H. Lowen, J. Phys. Condens. Matter 10 (1998) 6189.
[13] M. Schmidt, H. Lowen, Phys. Rev. E 55 (1997) 7228.
[14] H.J. Herrmann, G. Mantica, D. Bessis, Phys. Rev. Lett. 65 (1990) 3223.
[15] A. Kansal, S. Torquato, F.H. Stillinger, J. Chem. Phys. 117 (2002) 8212.
[16] E. Santiso, E.A. Muller, Mol. Phys. 100 (2002) 2461.
[17] N.N. Sinelnikov, M.A. Mazo, A.A. Berlin, J. Phys. I France 7 (1997) 247.
[18] D. Bideau, A. Gervois, L. Oger, J.P. Troadec, Journal De Physique 47 (1986) 1697.
[19] S.P. Ferguson, T.C. Hales, A Formulation of the Kepler Conjecture, University of Michigan, 1998.
[20] T.C. Hales, An Overview of the Kepler Conjecture, University of Michigan, 1998.
[21] L. Fejes Tóth, Regular Figures, The Macmillan Company, New York, 1964.
[22] D. Young, Computational Chemistry, Wiley, New York, 2001.
[23] J.B.M. Melissen, American Mathematical Monthly 100 (1993) 916.
[24] A. Florian, Ausfüllung der Ebene durch Kreise, Rend. Circ. Mat. Palermo 9 (1960) 1.
[25] S. Torquato, F.H. Stillinger, J. Phys. Chem. B 105 (11) (2001) 849.
[26] S. Torquato, A. Donev, F.H. Stillinger, Int. J. Solids Struct. 40 (2003) 7143.
[27] D. Levine, P.J. Steinhardt, Phys. Rev. B 34 (1986) 596.
[28] D. Shechtman, I. Blech, D. Gratias, J.W. Cahn, Phys. Rev. Lett. 53 (1984) 1951.
[29] K. Edagawa, K. Suzuki, S. Takeuchi, Phys. Rev. Lett. 85 (2000) 1674.
[30] P. Guyot, P. Kramer, M. de Boissieu, Rep. Prog. Phys. 54 (1991) 1373.